Scanning Microscopy

Volume 1990
Number 4 *Fundamental Electron and Ion Beam Interactions with Solids for Microscopy, Microanalysis, and Microlithography*

Article 8

1990

Monte Carlo Simulation of Secondary Electrons in Solids and its Application for Scanning Electron Microscopy

M. Kotera
Osaka Institute of Technology, Japan

T. Kishida
Osaka Institute of Technology, Japan

H. Suga
Osaka Institute of Technology, Japan

Scanning Microscopy Supplement 4, 1990 (Pages 111-126)
Scanning Microscopy International, Chicago (AMF O'Hare), IL 60666 USA

0892-953X/90$3.00+.00

MONTE CARLO SIMULATION OF SECONDARY ELECTRONS IN SOLIDS AND ITS APPLICATION FOR SCANNING ELECTRON MICROSCOPY

M. Kotera, T. Kishida, and H. Suga

Department of Electronic Engineering
Osaka Institute of Technology
Omiya, Asahi-ku, Osaka, Japan

Abstract

A new Monte Carlo calculation model is introduced to simulate not only the primary electron behavior but also the secondary electron cascade in a specimen bombarded with an electron beam. Either the primary or the generated electron in a specimen having energy greater than 0.1keV is defined as a fast electron and the single scattering model is used in the simulation which employs the Mott elastic scattering cross section and the Rao Sahib-Wittry energy loss equation. The electron having energy smaller than 0.1keV is defined as a slow electron and the cascade model is used which takes into account the classical binary collision with the conduction electrons. The performance of this simulation is verified in comparison with experiments for energy and angular distributions of slow secondary electrons (<50eV). Then, this simulation is applied in a discussion of the quantitative signal variation of the secondary and the backscattered electrons depending on a specimen surface topography. The maximum intensity of the secondary electron signal is obtained where the scanning electron beam reaches around 1nm beside the top edge of a surface step made of Cu with the vertical side wall of 500nm in height.

KEY WORDS: Secondary electron trajectory, Primary electron trajectory, Monte Carlo simulation, Electron cascade, The Mott cross section, Evaluation of topographic contrast.

Address for correspondence:
Masatoshi Kotera
Department of Electronic Engineering
Osaka Institute of Technology
5-16-1, Omiya, Asahi-ku
Osaka, 535, Japan
Phone No.: Japan/06/952/3131

Introduction

Image contrast of the scanning electron microscope (SEM) is produced arising from differences in emission yield of the secondary(SE) or the backscattered electrons(BSE) due to local features of topography, composition, electric field, etc. at the specimen surface. For quantitative analyses of the specimen feature using the contrast, it is necessary to have a deep understanding of the processes these electrons undergo in the specimen.

The theoretical studies have been made of processes involving SE generation, transport, and escape from the specimen's surface. The theories may be divided into four levels of approximation. The first assumes a simple empirical equation for SE emission and uses adjustable parameters for each material.[1,9,36,43] The second assumes an analytical model for the geometry of the electron diffusion, and yields the energy or the spatial distribution of SE emission.[14,15,24,35,38,39] The third uses mathematical expressions for generation and escape and employs the Boltzmann transport equation, to obtain several physical quantities of SE.[2,3,5,6,7,44,45,53] The fourth uses a simulation of electron trajectories in the specimen with Monte Carlo calculation. Every probability distribution to express each phenomenon electrons undergo in the specimen can be taken into account in the calculation. After calculation of a large number of trajectories the results are summed to obtain statistical values in various physical quantities of SE.[13,17,18,19,21,26,34] The theories become progressively more general in going from the first to the fourth.

Shimizu and Murata[48], Shimizu[49], George and Robinson[20], Murata et al.[37], and Joy[22] have used Monte Carlo calculations to simulate primary electron (PE) scattering in a specimen, and they deduced the SE emission intensity from the PE energy deposition near the surface of the specimen with considerable success. However, because they did not calculate each generated SE trajectory, it was primarily difficult to quantify the energy or the angular distribution of SE emission from the specimen surface.

Ganachaud and Cailler[17,19] and also their associates[13,18,21], Koshikawa and Shimizu[26], Koshikawa[27], Ding and Shimizu[16], and Luo and

Symbol Table

SEM	Scanning electron microscope
PE	Primary electron
SE	Secondary electron (the energy < 50eV)
BSE	Backscattered electron (the energy ≥ 50eV)
E	An electron energy in the specimen (eV)
E'	The energy of a scattered electron (eV)
N	The number of atoms per unit volume (cm^{-3})
e	The electronic charge (C)
Z	The atomic number
J	The mean ionization potential of an atom(eV)
c	The light velocity (cm/s)
m	The electron rest mass (g)
h	The Planck's constant divided by 2π (erg·s)
E_p	An energy of the fast electron (eV)
E_F	The Fermi energy (eV)
k_F	The wave vector at the Fermi energy (cm^{-1})
E_C	The surface potential barrier (eV)
s	Step length of a fast electron (cm)
λ_f	Elastic mean free path of a fast electron
λ_s	Inelastic mean free path of a slow electron
n	Index of refraction for a slow electron passing through the specimen surface
θ	The external angles of the electron trajectory measured from a normal to the surface.
θ'	The internal angle of the electron trajectory measured from a normal to the surface.
δ	Secondary yield
η	Backscattering yield
I(r)	Radial distribution of PE beam current density

Joy[34] have tried straight forward simulation of SE behavior in a specimen using Monte Carlo methods. All of their calculated results have shown good agreement with some fundamental experimental results eg. energy distribution, yield, and angular distribution of emitted SEs and BSEs. However, none of the papers except Koshikawa and Shimizu[26] have discussed the spatial distribution of those signals.

As is well known, a major mechanism in producing SE's in metals is the electron cascade process. Koshikawa and Shimizu[26] have taken into account only the cascade process, and show that the calculated results agreed very well with experimental results for the energy and the angular distribution of SE's at the specimen surface. Even though their approach uses rather coarse approximation, unless we are interested in fine structures found in electron energy loss spectrum, or Auger electron spectrum, their model is practically acceptable. We have to note, however, they assumed the PE moved along a straight line without energy loss. On the other hand, for electrons whose energy lies from several tens of keV down to 0.1keV, the trajectory is quite well described by a Monte Carlo simulation with the single scattering model, and various applications of the method have been reported in the field of SEM, electron probe micro-analyzer, electron beam lithography, etc.[20,22,28,29,33,37,41,42,48,49,50] A major insufficiency of this model occurs when the electron energy is low. This is because the accuracy of the Bethe theory which constitutes major part of the model becomes insufficient for electrons whose energy is less than about few keV or for heavy elements. Considering these advantages and disadvantages of these two types of the simulations and each applicable energy region, it should be very useful to combine these two models.

In the present study, either the primary or the generated electron in a specimen having energy greater than 0.1keV is defined as a fast electron and the single scattering model is used in the simulation which employs the Mott elastic scattering cross section and the Rao Sahib-Wittry energy loss equation. The electron having energy smaller than 0.1keV are defined as a slow electron and the cascade model is used which takes into account the classical binary collision with atomic electrons. The performance of this simulation is verified in comparison with experiments for energy and angular distributions of slow secondary electrons (<50eV).[30,31] Then, this simulation is applied in a discussion of the quantitative signal variation of SEs and BSEs at a specimen surface topography. The influence of SE and BSE signals, which are made at walls of the specimen chamber in the SEM because of high energy BSEs from the specimen, is not considered.

Simulation model

Fast Electrons

In the present simulation of fast electron scattering in a specimen, the electron energy loss is calculated by using the modified Bethe equation of Rao Sahib and Wittry[40], namely:

$$-\frac{dE}{ds} = \frac{2\pi e^4 N}{E}\ln\left(\frac{1.166E}{J}\right) \quad , \text{for } E \geq 6.338J \quad (1)$$

$$-\frac{dE}{ds} = \frac{2\pi e^4 N}{1.26(JE)^{1/2}} \quad , \text{for } E < 6.338J \quad (2)$$

where E is an electron energy, N is the number of atoms per unit volume, e is the electronic charge, Z is the atomic number, J is the mean ionization potential of the atom given by the equation of Berger and Seltzer[4]: $J = 9.76Z + 58.5Z^{-0.19}$ (eV).

For the elastic scattering cross section of an electron, the Mott cross section is used. This cross section is believed to remain accurate at low energies and for heavy elements[28]. The cross section per unit solid angle in a direction θ i.e. the differential cross section is expressed by the following equation for an unpolarized electron beam:

$$\frac{d\sigma}{d\Omega}(\theta) = |f(\theta)|^2 + |g(\theta)|^2 \quad (3)$$

The functions $f(\theta)$ and $g(\theta)$ are the scattering amplitudes which are given by the partial wave expansion analysis of the relativistic wave equation of Dirac[32] as follows.

$$f(\theta)=\frac{1}{2iK}\sum_{l=0}^{\infty}\{(l+1)[\exp(2i\delta_l)-1]+l[\exp(2i\delta_{-l-1})-1]\}P_l(\cos\theta) \quad (4)$$

$$g(\theta)=\frac{1}{2iK}\sum_{l=1}^{\infty}[-\exp(2i\delta_l)+\exp(2i\delta_{-l-1})]P^1_l(\cos\theta) \quad (5)$$

where $i = (-1)^{1/2}$, $K^2 = W^2 - 1$, W is the total energy of the incident electron, P_l and P^1_l are the l th ordinary and the associated Legendre functions, respectively, and δ_l is the phase shift for the l th partial wave. In a practical

calculation the summation is carried out as far as the following condition is satisfied; $|\delta_\kappa| \leq 10^{-3}$. The phase shift, according to Bunyan and Schonfelder[11], is given by

$$\tan\delta_\kappa = \frac{Kj_{l+1}(Kr) - j_l(Kr)[(W+1)\tan\phi_\kappa + (1+l+\kappa)/r]}{Kn_{l+1}(Kr) - n_l(Kr)[(W+1)\tan\phi_\kappa + (1+l+\kappa)/r]} \quad (6)$$

using atomic units where $\hbar = c = m = 1$. This expression should be evaluated at large radius r where the atomic potential V is negligible. Also, takes the value either $-l-1$ or l according to spin-up or spin-down, $j_l(Kr)$ and $n_l(Kr)$ are the Bessel and the Neumann functions, respectively. is obtained by solving the following differential equation.

$$\frac{d\phi_\kappa}{dr} = \frac{\kappa}{r}\sin 2\phi_\kappa + (W-V) - \cos 2\phi_\kappa \quad (7)$$

This equation is part of the Dirac equations for an electron in a central field.[11] For the atomic potential V, one can use the Thomas-Fermi[12], the Hartree[12], the Hartree-Fock[51], or the Thomas-Fermi-Dirac[8] potential. In the present calculation the Hartree-Fock potential is used for Cu, the Hartree potential is used for Au, and the modified-Hartree-Fock potential[29] is used for Al. For example, according to Strand and Bonham[51], the Hartree-Fock potential for free neutral Cu atom can be evaluated by the following analytical expression.

$$V(r) = -Ze^2 r^{-1} Z_p(r)/Z \quad (8)$$

where

$$Z_p(r)/Z = \sum_{i=1}^{2} a_{\gamma i}\exp(-a_{\lambda i} r) + r\sum_{j=1}^{3} \cdot b_{\gamma j}\exp(-b_{\lambda j} r) \quad (9)$$

and

$$a_{\gamma 1}=1.5436,\ a_{\lambda 1}=3.856,\ a_{\gamma 2}=-0.5436,\ a_{\lambda 2}=47.41,\ b_{\gamma 1}=-8.439,\ b_{\lambda 1}=9.935,\ b_{\gamma 2}=-16.284,\ b_{\lambda 2}=32.013,\ b_{\gamma 3}=0.1973,\ b_{\lambda 3}=1.4838. \quad (10)$$

In a practical calculation of the scattering cross section, we introduced the functions $E(\theta)$ and $H(\theta)$[10] in stead of $f(\theta)$ and $g(\theta)$ which are defined by the following equations in the same manner done by Yamazaki[54]:

$$4iH(\theta) = \sum_{l=1}^{\infty}[\exp(2i\delta_{-l}) - \exp(2i\delta_l)]L^{-}_{l}(\cos\theta) \quad (11)$$

$$4iE(\theta) = \sum_{l=1}^{\infty}[\exp(2i\delta_{-l}) + \exp(2i\delta_l) - 2]L^{+}_{l}(\cos\theta) \quad (12)$$

where,

$$L^{\pm}_{n}(\cos\theta) = n[P_n(\cos\theta) \pm P_{n-1}(\cos\theta)] \quad (13)$$

Then, the cross section is expressed as

$$\frac{d\sigma}{d\Omega}(\theta) = \frac{1}{K^2}\left(\sec^2\frac{\theta}{2}\cdot|E|^2 + \operatorname{cosec}^2\frac{\theta}{2}\cdot|H|^2\right) \quad (14)$$

Equation (14) is calculated numerically, and the differential cross sections are listed in a table for many electron energies. The cross section at an energy of interest can be obtained by an interpolation from the values in the table.

The Bessel, the Neumann and the Legendre functions are calculated using recurrence relations as,

$$j_{m+1}(x) = -j_{m-1}(x) + (2m+1)\cdot j_m(x)/x \quad (15)$$

$$n_{m+1}(x) = -n_{m-1}(x) + (2m+1)\cdot n_m(x)/x \quad (16)$$

with initial conditions

$$j_0 = \sin x/x,\ j_1(x) = \sin x/x^2 - \cos x/x \quad (17)$$

$$n_0 = -\cos x/x,\ n_1(x) = -\cos x/x^2 - \sin x/x \quad (18)$$

and

$$L^{\pm}_{n+1}(x) = [(2n+1)xL^{\pm}_{n}(x) - (n+1)L^{\pm}_{n-1}(x) - (1\pm x)P_{n-1}]/n \quad (19)$$

$$P_{n+1}(x) = [(2n+1)xP_n(x) - nP_{n-1}(x)]/(n+1) \quad (20)$$

with initial conditions,

$$L^{\pm}_{0}(x) = 0,\quad L^{\pm}_{1}(x) = x\pm 1 \quad (21)$$

$$P_0(x) = 1,\quad P_1(x) = x \quad (22)$$

respectively.

These elastic and inelastic basic equations are combined in the single scattering model[28,29]. Electrons are assumed to loose their energy along the path continuously according to Eqs.(1) and (2). A change in direction of electron motion is assumed to be caused by elastic scattering events only for fast electrons, and this is calculated using Eq.(3). Therefore, the trajectory is divided into many steps, with step length basically equal to the mean free path λ_f for elastic scattering. In order to take account of variation in step length s, the step length s is calculated using a uniform random number R_S distributed from 0 to 1 as given by the following:

$$s = -\lambda_f \cdot \ln R_S \quad (23)$$

The electron trajectory of the fast electron is simulated until the electron escapes from the surface, or until its energy falls to 0.1keV.

Slow Electrons

The calculation model for slow electrons is basically the same as proposed by Koshikawa and Shimizu.[26] For the SE excitation function, the Streitwolf equation[52] is used, namely:

$$S(E) = e^4 k_F{}^3/(3\pi\cdot E_P(E-E_F)^2) \quad (24)$$

where E_P is an energy of the fast electron, E_F is the Fermi energy, and k_F is the wave vector at the Fermi energy. In this equation, S(E) is the number of SEs excited per unit energy into an energy interval between E and E+dE per unit path length of the fast electron (units of $cm^{-1}\cdot eV^{-1}$). In a practical calculation this energy distribution is obtained numerically by using random numbers. By taking the minimum and the maximum electron energy to be $E_C = E_F + \phi$ and E_P, respectively, the SE energy is given by using the uniform random number R_E, i.e.

Table I. Parameters used for Al, Cu, and Au in the present calculation.

	Work Function (eV)	Fermi Energy (eV)	Surface Potential Barrier (eV)	Number of SE Generated (PE= 1 keV)
Al	4.25	11.80	16.05	58.5
Cu	4.45	7.00	11.45	25.8
Au	4.25	5.51	9.76	30.0

$$E = (R_E \cdot E_F - A \cdot E_C) / (R_E - A) \qquad (25)$$

where $A = (E_P - E_F) / (E_P - E_C)$, ϕ is the work function and E_C is the surface potential barrier. The minimum energy E_C indicates that the calculation of slow electron trajectory continues until the electron energy becomes equal to E_C. Energies less than this are of no interest in the present case. The values of E_F, ϕ, and E_C for Al, Cu, and Au are summarized in Table I.

The angular distribution of a SE excitation by a fast electron is assumed to be spherically symmetric. The position of the excitation is determined at random within one step of the fast electron's trajectory. In a collision between a liberated SE and an electron of the specimen, the binding energy of the atomic electron is neglected, and the classical binary collision model is adopted. Then, the electron energy after the collision is $E'=E\cdot\cos^2\theta$, where θ is the scattering angle, and the energy of the other electron is $E''=E\cdot\sin^2\theta$. According to the assumption of spherically symmetric scattering in the center of mass system, taking into account the exclusion principle and the motion of the atomic electrons, Wolff showed that the average electron energy after scattering E' is related to the energy before scattering E as follows[53]:

$$E' = \alpha(E) \cdot E \qquad (26)$$

In this equation $\alpha(E)$ is nearly constant for $E \gtrsim 2 E_F$ according to Wolff. Therefore, we will consider $\alpha(E)$ to be a constant α over all the energy range of interest. Using the uniform random number R_C, the energy of a scattered electron E' is obtained from the following equation as used in Ref.[26]:

$$E' = E \cdot R_C^{1/2} \qquad (27)$$

After E' is determined in Eq.(27), the scattering angle of this slow electron θ_s is obtained. The mean free path for this collision process is determined from the following equation.

$$\lambda_s = 10^{(-2.6\cdot\log E + 3.3)} \text{ nm} \quad (E \leq 25\text{eV})$$

$$\lambda_s = 0.5 \text{ nm} \quad (25\text{eV} < E \leq 100\text{eV}) \qquad (28)$$

This equation was also introduced by Koshikawa and Shimizu[26] who have approximated experimental results for the escape depth of Auger electrons,

Table II. The classification of electrons in the present simulation model.

Electron energy	Definition	Simulation model	Electrons emitted from surface	Reentry of emitted electrons
$E_C \leq E < 50$eV	slow electron	cascade	SE	not considered
$50\text{eV} \leq E < 100$eV	slow electron	cascade	BSE	considered
$100\text{eV} \leq E$	fast electron	single scattering	BSE	considered

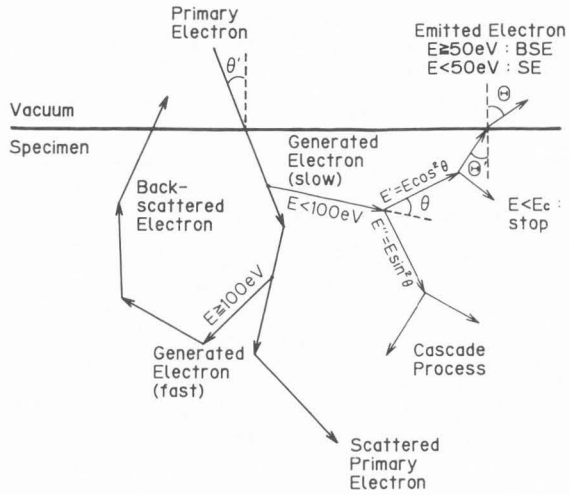

Fig.1. Schematic diagram of the present simulation model. The generated electron within the specimen may be a fast or a slow electron depending on whether the energy is above or below 100eV, respectively. The emitted electron from the specimen surface may be BSE or SE depending on whether the energy is above or below 50eV, respectively.

thus, the expression of Eq.(28) takes into account all the energy loss processes an electron will undergo in the specimen. The step length of a simulated SE is determined by considering its straggling from the mean value as in Eq.(23). The refraction of an electron trajectory at the specimen surface because of the potential barrier is calculated by the momentum conservation law. The index of refraction n is given by

$$n = \sin\theta / \sin\theta' = (E / (E - E_C))^{1/2} \qquad (29)$$

where E is an electron energy in the specimen, and E_C is the surface potential barrier. θ and θ' are the external and internal angles of the electron motion measured from a normal to the surface.

Fig.1 illustrates the present simulation model of fast and slow electron behaviors in a specimen. According to Table II, one of the two models is applied to simulate the electron trajectory, and the emitted electrons may be SE or BSE depending on the electron energy. Fig.2 shows an example of trajectories calculated by the present model of one PE incident normally on a bulk Cu specimen at 6keV. In this figure one can see a

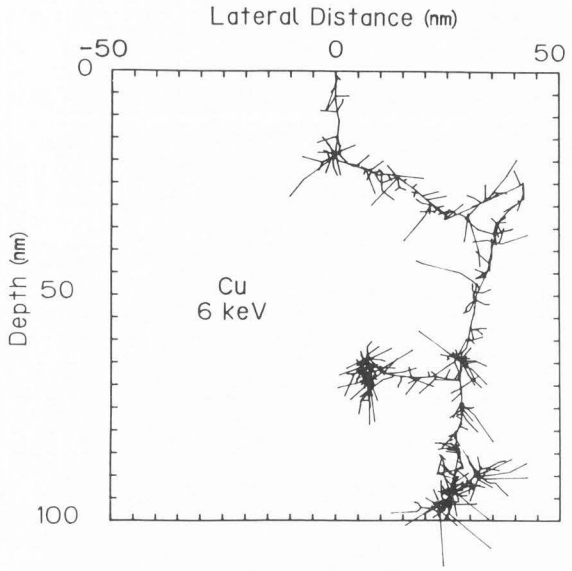

Fig.2. An example of simulated trajectories of one PE and generated fast and slow electrons in a bulk Cu specimen for 6keV PE incident normal to the surface.

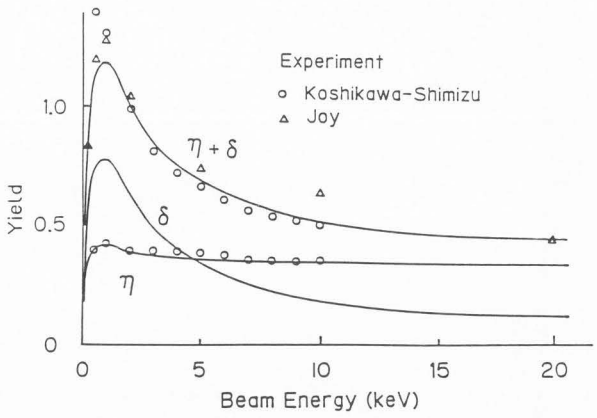

Fig.3. PE energy dependence of secondary yield at normal incidence to Cu surface. $\eta + \delta$: total secondary yield, η: backscattering yield (it consists of real backscattered PEs and high energy ($50 \leq E \leq 100$eV) slow electrons), and δ: real secondary yield (it consists of low energy ($0 \leq E < 50$eV) slow electrons).

meandering trajectory of the PE, also the SE cascades along it. In this sample calculation, one can see a high energy SE generated in the middle of the PE trajectory and it also has a meandering trajectory, with a ternary electron cascade taking place along that trajectory. The number of SE generated by the PE increases as the trajectory approaches the end of its range. For a slow electron the step becomes longer as the electron's energy becomes lower as expected from Eq.(28); here, long straight lines in the figure are the steps of low energy electrons. Since every fast electron loses its energy until 0.1keV and becomes a slow electron, one can see a cascade at the end of every fast electron trajectory.

Number of SE Generation

Although S(E) in Eq.(24) gives an absolute number of SE excitations in one PE trajectory, contributions of plasmon and Auger electrons to the SE production are not taken into account. Also in the present calculation model of electron cascade, only binary collision is considered as a process slow electrons undergo. In order to compensate for these insufficiencies of the present treatment, S(E) is regarded here as a relative value. The number of SE generated by each PE is adjusted in the present model, and this is determined by a comparison with experimental results. Experimental results of Koshikawa and Shimizu[25] show that the total secondary yield from the specimen surface is about 1.0 for 2keV PE incident on Cu, and the simulation is set to give the same value. A tentative value for the total number of SE generated by a 1keV PE is 25.8, if the PE trajectory lies entirely within the specimen. Of course the average number of SE generated in the specimen is less than this value because of the PE backscattering. The value of 25.8 is adopted to match the calculated results considering the backscattered PE and the low energy SE emission from the specimen's surface with experimental results. Since it is assumed that only electrons over 0.1keV can produce SEs, the number of SE generated in one step of the PE trajectory, if it is in the specimen, is calculated simply by the following equation:

$$\frac{25.8 \cdot (\text{PE energy loss in a step in keV})}{(\ 1.0 - 0.1\ )} \qquad (30)$$

The total number of SE generated for a PE at E_0keV is $25.8 \cdot (E_0 - 0.1)/(1.0 - 0.1)$ in one trajectory. Neglecting 0.1keV compared to E_0 in this equation, a 10keV PE produces basically 10 times more SE than a 1keV PE in the specimen. In the same manner the number of SE's generated at 1keV PE incident on Al and Au is summarized in Table I.

It should be noted that the energy conservation law is not satisfied in the present simulation. For example, when a fast SE is generated from the PE trajectory, the energy loss of the PE due to the ionization is not considered. Therefore, the backscattering yield obtained by the present calculation becomes larger than the previously calculated result using the single scattering model because of the increased emission of the generated fast secondary electrons along PEs. Also, the mechanism of SE production by plasmons should be treated more precisely which has a significant influence on the SE excitations. These aspects of the problem should be treated in a future study.

Results and discussions

According to the usual convention if an electron emitted from the specimen surface has an energy greater than 50eV, it is considered a backscattered electron (BSE); if it has an energy less than 50eV, it taken as a SE. These classifications are summarized in Table II.

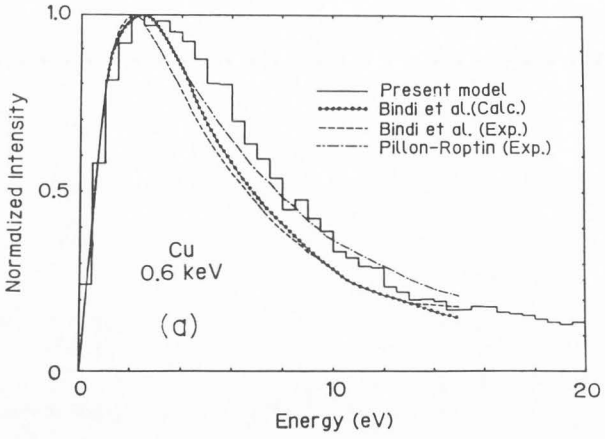

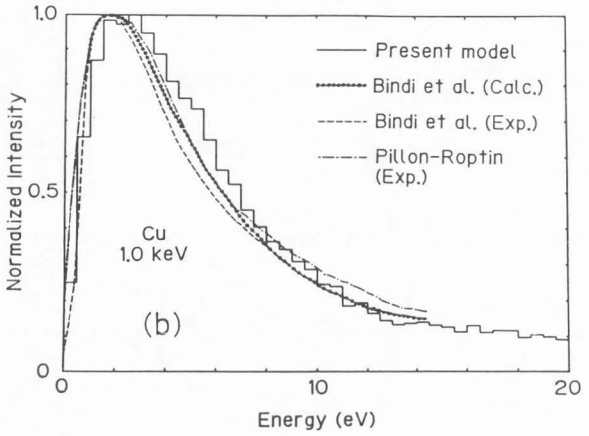

Fig.4. Normalized energy distributions of emitted SE from Cu for (a)0.6keV and (b)1.0keV PE. "Calc." and "Exp." show the calculated and the experimental results, respectively. Experimental results of Pillon and Roptin are quoted from a paper of Bindi et al.[5]

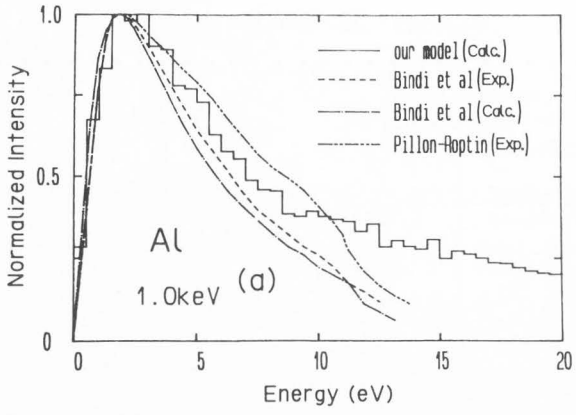

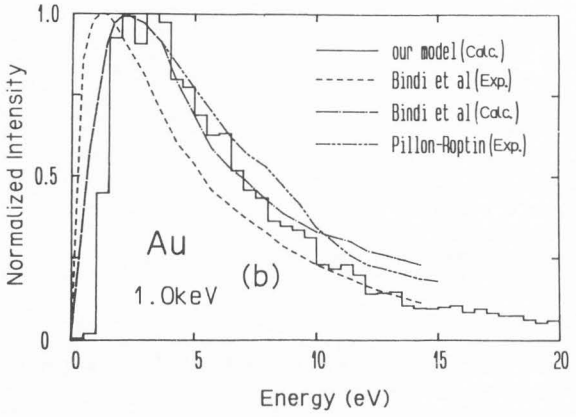

Fig.5. Normalized energy distributions of emitted SEs from Al and Au specimens at 1keV PE incidence. "Calc." and "Exp." show the calculated and the experimental results, respectively. Experimental results of Pillon and Roptin are quoted from a paper of Bindi et al.[5]

Secondary and Backscattering Yields

The total yield at 2keV PE incidence is adjusted to agree with the experimental result of Koshikawa and Shimizu.[25] With this adjustment, the calculated total secondary yield from the specimen ($\eta+\delta$) agrees quite well with experimental results of Koshikawa and Shimizu[25] and Joy[22] over a wide range of energy as shown in Fig.3. Taking the ratio of the number of electrons emitted from the specimen surface whose energy is higher than 50eV to the number of the incident electrons, the backscattering yield (η) is obtained. In the same manner the ratio of the number of emitted electrons from the specimen surface whose energy is less than 50eV to the number of the incident electrons is the secondary yield (δ). The energy dependence of the backscattering yield (η) is plotted in the figure, and again, very good agreement is found between the calculated result and the experimental result. A small hump is observed at around 1keV for the backscattering yield. This is because of an influence of high energy slow electrons as follows. Not only backscattered PEs, but also high energy slow electrons ranging from 50eV to 100eV are counted as backscattered electrons. Because the yield of low energy (<50eV) electrons δ increases rapidly at low PE energies as shown in Fig.3, the number of high energy (≥50eV) slow electrons, which is included in the BSE, should increase for this PE energy. Since the calculated distributions of $\eta+\delta$ and η agree with the experimental results quite well, the distribution of real secondary yield δ should be very close to the real one.

Energy Distribution

Energy distributions of SE are shown in Figs.4(a) and (b) at 0.6 and 1.0keV PE incident normally on a bulk Cu specimen. They are normalized to have the same peak value. The calculated results are shown in the histogram. The experimental and the other theoretical values are quoted from a paper of Bindi et al.[5] The calculated result of Bindi et al. has been obtained based on the Boltzmann transport equation. The present results show good agreement with the other results shown in Fig.4. However, the peak energy is a little higher and the full width at half maximum of the distribution is a little larger for the present work compared to the other distributions. The difference is larger at the lower PE energy.

In an analysis of SE emission by Koshikawa and Shimizu[26], the maximum escape depth of SE is about 7.5nm in Cu. Since the extrapolated electron range for 1keV PE is about 10.0nm and the energy deposition has a peak at some depth, the SE generation is not uniform within the escape depth. If a SE is generated at a shallow region from the surface, the SE can keep its generation energy with high probability in its transport toward the surface, then a contribution of high energy SE to the energy distribution is increased. On the other hand, for high energy PE incidence, PE penetrates through a layer of 7.5nm in a few initial steps and the spatial spread is very small. Then, the SE generation is quite uniform in the escape depth. In this situation the relative probability of the lower energy SE emission from the surface is increased. This is the reason that the calculated peak shifts toward higher energy and the distribution becomes wider for lower energy PEs. The electron beam energy dependence of the SE energy distribution is also found in the curves obtained experimentally by Koshikawa and Shimizu,[25] and Bindi et al.[5]

In the same manner, calculation is made for Al and Au specimens with the parameter shown in Table I. The energy distribution of SE for Al and Au is shown in Fig.5 when the incident PE energy is 1keV. Although the present calculation model does not include plasmon excitation, inner-shell excitation, and some other processes which electrons undergo in the specimen, the calculated distribution agree quite well with calculated results of Bindi et al.[5,6] and other experimental results. The calculated distribution of Al shows wider distribution than that of Au. This is because the surface potential E_C is smaller for Au. The relative probability of electron generation increases rapidly with decreasing electron energy as understood by Eq.(24), and if E_C is small, the energy distribution of generated slow electrons are peaked sharply and the energy distribution is getting narrower.

Spatial Distribution

Here, the Gaussian spatial distribution is assumed for the PE beam current density as expressed by the following:

$$I(r) = I(0) \cdot \exp(-(r/\xi)^2) \qquad (31)$$

Here, the beam diameter 2ξ is set 0.1nm. A spatial distribution of SE or BSE can be clarified by the difference between the distribution and the original Gaussian distribution. This assumption makes it easier to quantify the emission region of signals. The radial distributions of SE and BSE for 1 and 10keV PE incidence are shown in Fig.6. These distributions show the theoretical resolution of the SEM image.

It should be noted that the region shown in Fig.6 by the distribution is very narrow compared to the electron range (for example, about 10.0nm in Cu at 1keV). Therefore, this distribution is produced mainly by the influence of the initial few steps of the simulated incident PE, and the contribution of the PE backscattering after the deep penetration in the specimen is very low. Thus, the SE intensity is mainly determined by the amount of the PE energy loss in the maximum SE escape depth from the specimen surface. Also,

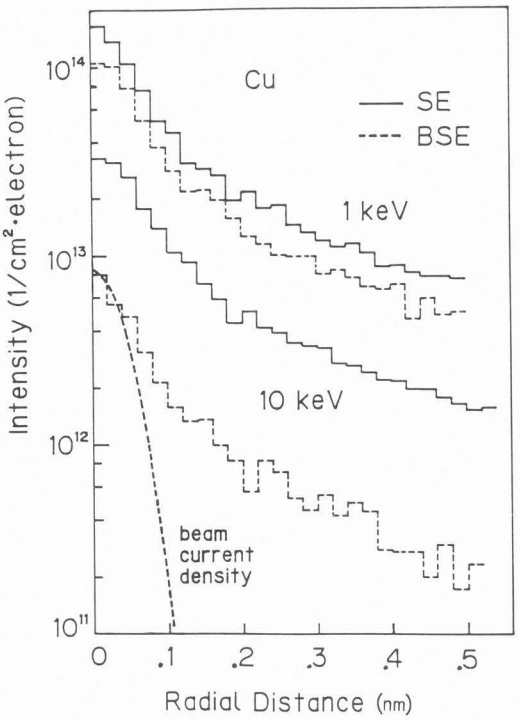

Fig.6. Radial distributions of emitted BSE and SE from Cu surface for (a)1keV and (b)10keV PE. Broken line shows the Gaussian current density distribution assumed here for the PE beam.

the BSE intensity is mainly determined by the Mott differential cross section at the scattering angle over 90 degree. Some features for SE and BSE are shown in the figure. The diameter at half intensity of the peak value for the beam center can be referred as the emission region of the signal. Since the slope of the distribution for SE is more gentle than that of BSE, the following discussion can be made. The emission region of SE is wider than that of the BSE for both PE energies. Since the energy of the BSE should be low at some distance from the PE incident point, (1).a lower energy BSE can produce more SEs effectively, and (2).a BSE will be recognized as a SE if its energy is less than 50eV. (3).The generated SE itself can spread out in a wide range. The SE mean free path increases with decreasing energy, as shown in Eq.(24), and the mean free path is 3.525nm at the threshold energy to overcome the surface potential of Cu (11.45eV).

Both signals decrease as the PE energy increases. For BSE it can be understood by the fact that the Mott cross section for high backscattering angles at 10keV is much smaller than that of 1keV as shown in Fig.7. On the other hand, according to the Rao Sahib and Wittry equation (Eq.(2)) the energy loss is in proportion to $E^{-0.5}$, and this is because the SE intensity decreases at high incident energy as in Fig.6. Although the absolute intensity for SE seems to be higher than that of BSE and the difference increases with energy in the figure, it is not always true and these distributions cross at 0.6keV PE incidence. However, the relative variation of each radial distribution of SE is

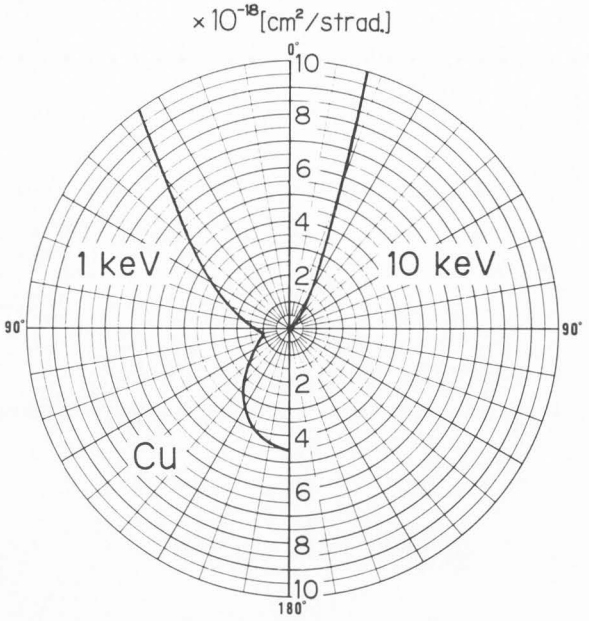

Fig.7. The Mott differential cross section for Cu at 1keV and 10keV in the polar plot.

almost independent of the PE energy.

Usually it is assumed that the full width at half maximum of the spatial distribution of SE intensity is of the order of the mean free path of SE,[14,26] and for Cu it is from 0.5 to 2.0nm.[46] The present result shows that the diameter at half maximum of the distribution for BSE is 0.130nm and 0.118nm for 2ξ=0.1nm PE beam energies of 1 and 10keV, respectively. For SE each of them is 0.125nm and 0.157nm, respectively. Although present values are much smaller than the value previously believed, a fairly large contribution to the SE emission comes from the tail of the distribution.

It is generally believed that the resolution of an SE image is much better than that of a BSE image in the SEM, but the present calculation shows the opposite tendency at 10keV. Although the present calculated result shows a theoretical signal distribution, no surface feature is taken into account, such as topographic, compositional, and electric potential differences. The signal variation for SE and BSE at some topographic feature of the specimen will be discussed later.

Angular distribution of emitted SE and BSE

The calculated angular distribution of emitted BSE and SE intensities from a Cu surface at normal PE incidence are shown in a polar plot as a function of scattering angle in Fig.8(a) and (b) for 1 and 10keV PE, respectively. Generally, the angular distributions of BSE and SE are coincident with a cosine function, which is shown in a solid line in the figure. At around $\theta = 0°$ the integrated solid angle by the azimuthal angle is small, and the statistics of the electron detection is not sufficient. Assuming that the detected number of BSE or SE is M_1, the amount of the error should be $(1/M_1)^{1/2}$, and this value is shown in a error bar in Fig.8. It is found that the variations of SE at 1keV and BSE at 10keV agree

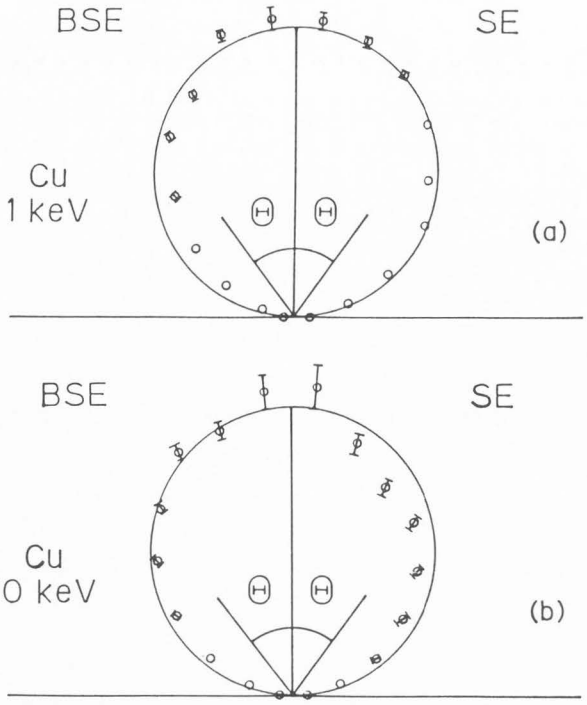

Fig.8. Angular distributions shown in a polar plot for emitted BSE and SE from Cu at (a)1.0keV and (b)10keV PE incident normal to the surface. The statistical error is shown in the bar. The cosine distribution is shown in a solid line.

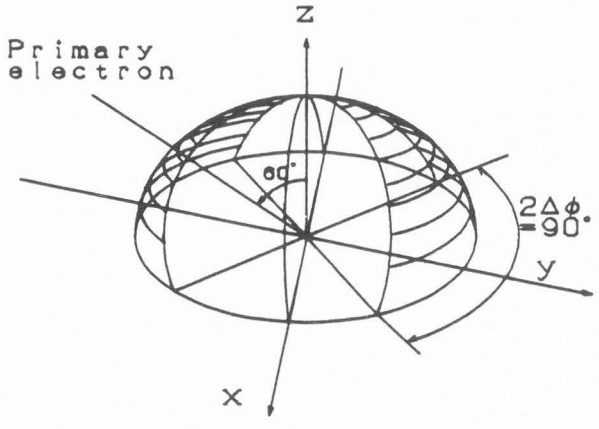

Fig.9. Schematic diagram of the solid angle for SE and BSE detection at PE oblique incidence.

with the cosine law. In the variations of BSE at 1keV and SE at 10keV, the distributions are more peaked in a direction normal to the surface than the cosine function. This variation for BSE at 1keV can be attributed to the Mott elastic scattering cross section as discussed in the next paragraph.

The angular distribution of emitted BSEs and SEs at oblique incidence of PE on the specimen are also calculated. A geometrical diagram of the calculation is shown in Fig.9. The x-y plane is the specimen surface. The incident PE beam is in

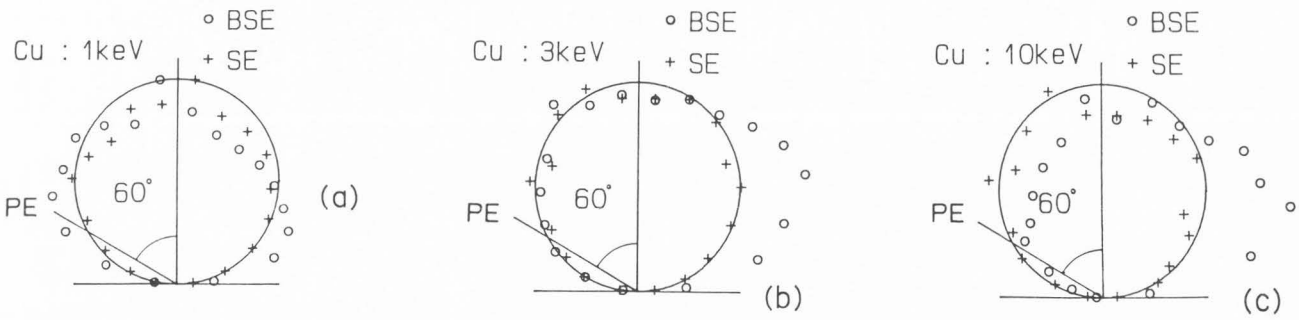

Fig.10. Angular distributions shown in a polar plot for emitted BSE and SE from Cu at (a)1.0keV, (b)3keV, and (c)10keV PE incident at 60 degree from the normal angle to the surface.

the y-z plane. For oblique incidence the BSEs are counted only in the shaded part of a spherical coordinate system (θ = 60°, $-45° \leq \phi \leq 45°$). The calculated results are shown in the polar plot for 1, 3, and 10keV PE incident on Cu in Fig.10. For BSEs at 3 and 10keV PE the distribution is peaked at the reflective angle of the PE incidence, but at 1keV PE incidence the distribution is peaked not only at the reflective angle but also at the incident angle. This angular dependence is because of the Mott differential cross section used in the calculation of the fast electron elastic scatterings. As shown in Fig.7, the Mott cross section of high backward scattering angles at 1keV is much larger than that at 10keV. On the other hand, the angular distribution of SE emission from Cu at every PE energy is almost independent of the PE incident angle as shown in Fig.10, and it agrees with the cosine function. This phenomenon has already been found experimentally as pointed out by Seiler.[47]

SE and BSE yield as a function of the angle of PE incidence

All signal intensities are expressed in terms of yield, the ratio of the number of emitted electrons (SEs or BSEs) to the number of incident PEs.

Oblique infinite plane First, the intensity variation of BSE and SE signals with oblique angle of the specimen surface to the PE incidence is calculated. Fig.11 shows an illustration of the boundary condition of the specimen. The thickness and the area of the surface are infinitely large. The oblique angle of the plane equals PE incident angle taken from the normal to the specimen surface.

The change in the coefficients of escape according to the angle of incidence is examined for an incident energy of 1 and 3keV, as shown in the right part of Figs.12(a) and (b), respectively. The value of η is the ratio of the number of BSEs to that of PEs (= the backscattering coefficient), δ is the ratio of the number of SEs to that of the PEs. The solid line in this figure shows the data obtained by the experiment of Koshikawa and Shimizu,[25] while the broken line indicates the data obtained by the experiment of Muller quoted from the paper of Koshikawa and Shimizu.[25] The results of our calculation agree well with these experiments. The dependence of

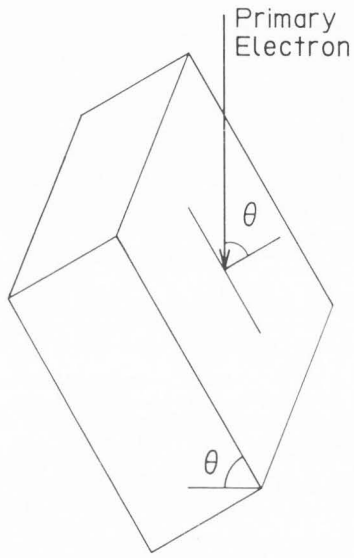

Fig.11. Illustration of the oblique infinite plane specimen made of Cu.

η, δ, and $\eta+\delta$ on the PE incident angle is generally thought to be coincident with the secant function. An approximately similar tendency is seen in the present result. The distribution indicated by a dotted line is the secant distribution normalized at θ = 0. In the present calculation, the increasing rate of η and δ at higher angles is smaller than that of the secant distribution. Koshikawa[27] reported that the values of these coefficients were smaller than those determined by the secant law at large angle incidence of PEs if the atomic number of the specimen was higher than that of Al (e.g. Cu), and that they were larger than the values determined by the secant law at large angle if the atomic number was low.

At an incident energy over 1keV, the value of δ at θ=0 becomes smaller as the incident energy becomes larger. This is because the number of SEs excited is approximately proportional to the amount of energy loss of PEs within the maximum escape depth of SEs (e.g. 10nm). According to the Rao Sahib and Wittry equation, the energy loss is proportional to $E^{-0.5}$ if E is less than 6.338J=1.989keV in Cu, that is, the energy loss becomes larger as the incident energy becomes smaller.

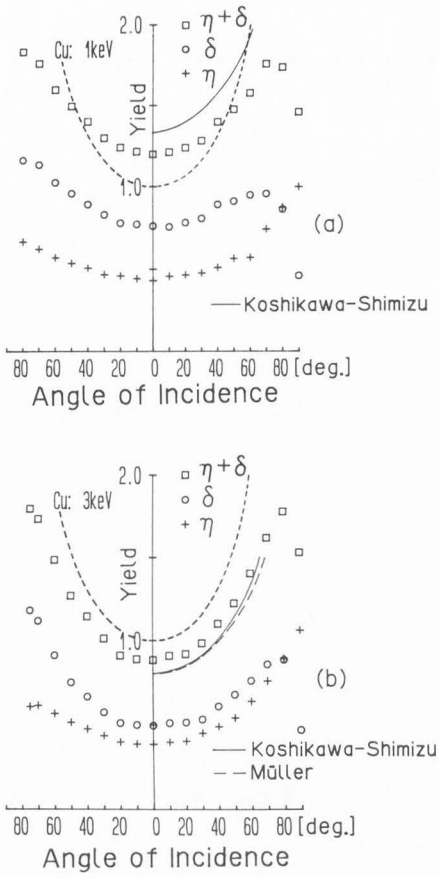

Fig.12. Electron yields of SE and BSE as a function of incident angle of PEs, for (a):1keV and (b):3keV. $\delta + \eta$: total SE yield, δ: SE yield, η: BSE yield. The experimental curve of Muller is quoted from the paper of Koshikawa and Shimizu.[25]

The calculated value of δ decreases sharply at very large angle, especially when the energy is low. This is because when the incident angle is so large, most of the PEs which could excite SEs with diffusing within the maximum escape depth of SEs, escape as BSEs immediately after the bombardment of the specimen surface. In such situation the source of SE production decreases with increasing the PE incident angle.

Wide oblique plane followed by infinite horizontal plane Fig.13 shows an illustration of the pattern used in this calculation. The thickness is infinite, and the area of the horizontal plane is infinitely large in the calculation. The difference in height between the top edge of the oblique plane and the horizontal plane surface is 500nm so that escape of electrons from the upper edge of the pattern or creeping of electrons under the join of planes due to scattering might be avoided. Electrons are irradiated onto the central region of the oblique area.

Here, we can estimate the influence of SEs made after the BSE reentry on the horizontal plane area as illustrated in Fig.13. The signal intensity at the irradiation of PEs onto the oblique plane of this pattern is compared with the signal intensity for an incidence of electrons onto the oblique infinite plane described in the

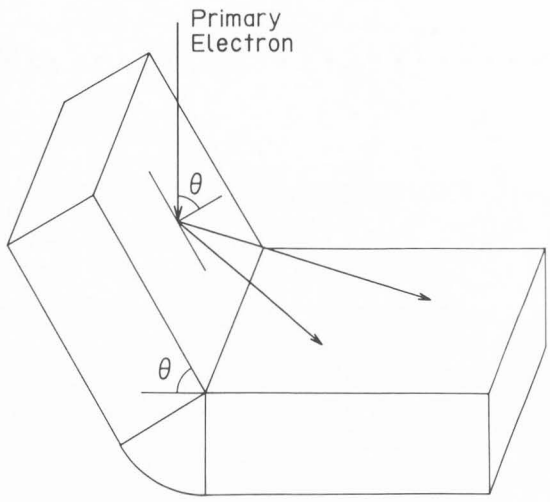

Fig.13. Illustration of wide oblique plane followed by infinite horizontal plane made of Cu. Some of PEs incident vertically onto the oblique area are reflected as BSEs and reenter the horizontal area of the specimen, and the BSEs generated at the horizontal area will re-reenter the oblique area. Calculation is made for taking into account all these processes.

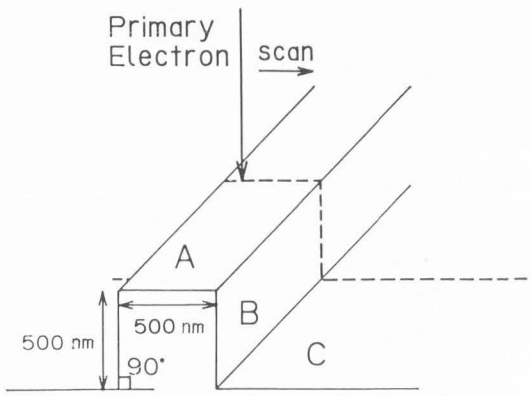

Fig.14. Illustration of a convex step with vertical side walls on the infinite horizontal plane. PE beam incident vertically on the specimen is scanned across the step. With varying the width of the step the SE and BSE signals are examined. In the simulation, all trajectory of BSE is calculated even after its emission from the specimen surface, and if it is pointing to other part of the surface, we let the BSE incident onto the specimen and trace the trajectory.

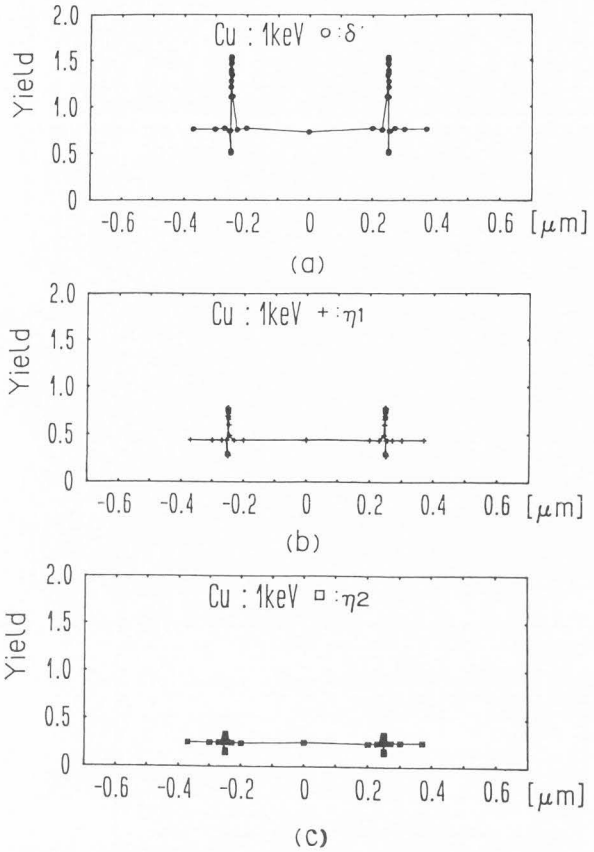

Fig.15. Signal waveforms of emitted all SEs (δ) and emitted all BSEs (η_1) and the detected BSEs (η_2) for the illustrated pattern in Fig.14 with L= 500nm for 1keV PE.

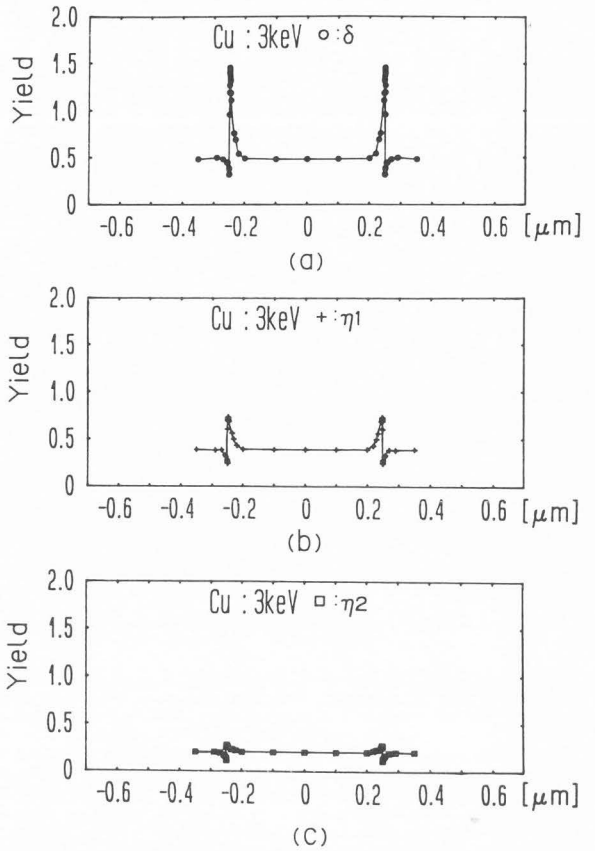

Fig.16. Signal waveforms of emitted all SEs (δ) and emitted all BSEs (η_1) and the detected BSEs (η_2) for the illustrated pattern in Fig.14 with L= 500nm for 3keV PE.

last paragraph. The difference in the signal is attributed to the reentry of electrons onto the horizontal plane as illustrated in Fig.13. The left part of Fig.12 shows the escape coefficient of SEs (δ) and the backscattering coefficient (η) and the total yield ($\eta+\delta$) at different tilt angles (θ) of the specimen under the setting mentioned above. To compare the values of these coefficients under these settings with those obtained for PE incidence onto the oblique infinite plane, the number of SEs is larger in the former than in the latter. Under the boundary condition shown in Fig.13, PE emission at the reflective angle is emphasized, and the probability of the electron reentry onto the horizontal plane area is increased. Therefore, not only the SEs excited in the oblique area but also the SE excited in the horizontal area after the reentry are released from the specimen as signals. On the other hand, the number of BSEs is smaller than the value on the infinite plane. The contribution of PE reentry onto the horizontal plane to the BSE signal is small for the following two reasons: (1)the backscattering coefficient for the electrons incident on the specimen is usually smaller than unity, if we assume that all of the reflected PEs at the oblique area show the reentry, the backscattering coefficient can be expressed by η^2 with neglecting its energy and angular dependences. Therefore, the contribution of PE reentry onto the specimen to the BSE yield is very small. (2)It is highly probable that the electron cannot keep its energy as BSE due to energy loss after the reentry onto the horizontal plane.

The difference between the right part and the left part of Fig.12 for both coefficients of η and δ becomes large according to the tilt angle. This is also understandable if we remember that the reentry of electrons occurs more easily at higher tilt angles because of increased reflective scattering at the specimen surface.

This phenomenon is also depending on the PE incident energy as seen in a comparison between the results shown in Figs.12(a) and (b). The rate of variance becomes larger at high incident energy than at low energy. This is because the forward scattering of PEs increase at higher energy according to the Mott cross section, resulting in an increased probability for them to escape out of the oblique area in the reflection angle.

Analysis of the edge effect

On the basis of the knowledge of SE and BSE signal intensities as discussed above, a topographic signal contrast in the SEM is discussed in this paragraph. The resolution of the SEM depends on the shape of the topographic patterns. Here, we assume a convex step pattern

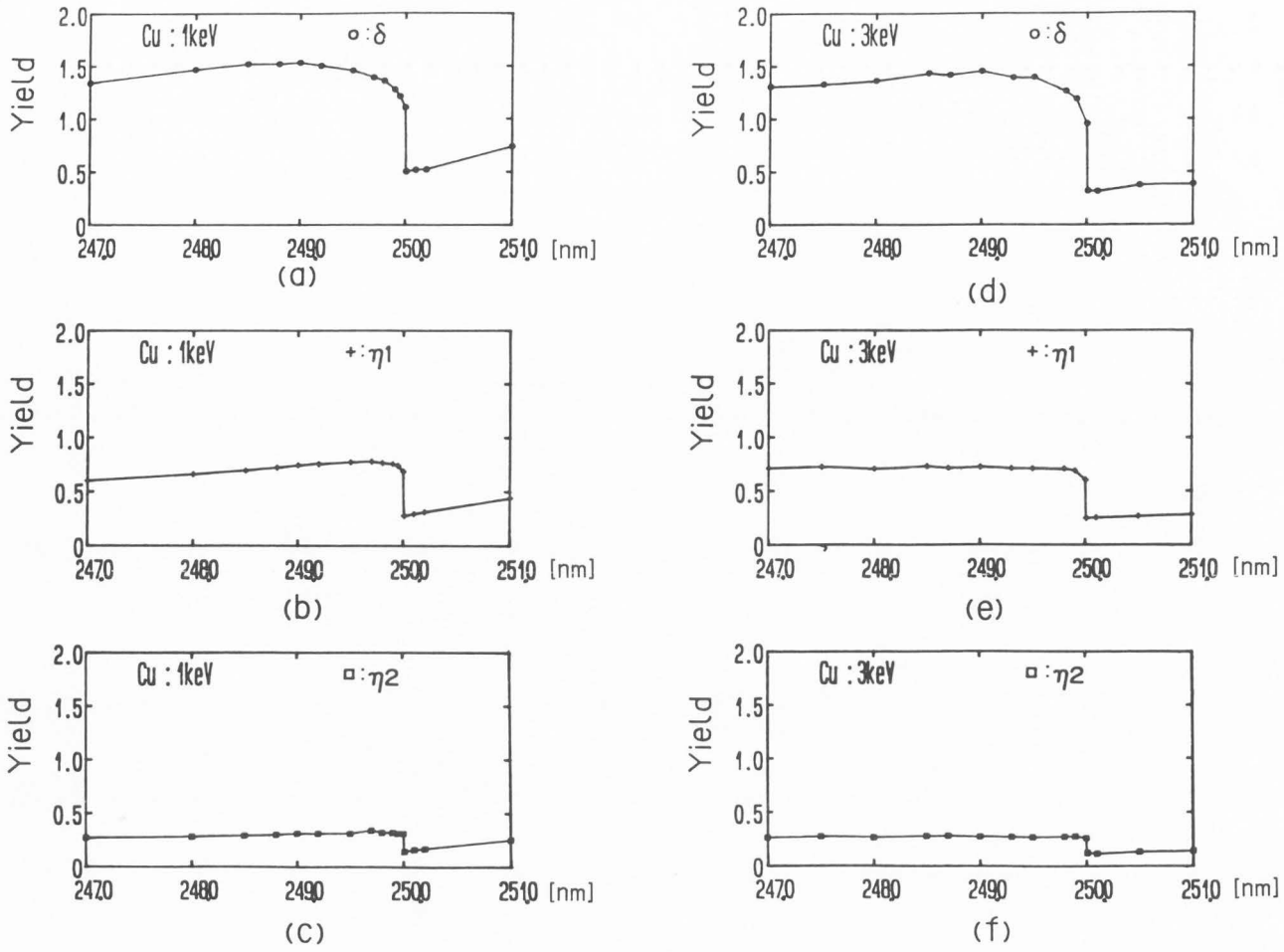

Fig.17. Signal waveforms in the vicinity of the edge of the convex step pattern expressed in Fig.16 pattern with vertical side wall. (a)-(c): 1keV PE, (d)-(f): 3keV PE.

with vertical side walls on the infinitely large horizontal plane as illustrated in Fig.14. This specimen consists of three characteristic portions, and we call them A, B, and C as in the figure. Its height is 500nm, and the width of the upper portion (A) is also 500nm. and the SE and the BSE signal intensities are calculated as PE is scanned across this convex step pattern.

Figs.15(a-c) and Figs.16(a-c) show the signal waveforms for each pattern at incident electron energies of 1 and 3keV, respectively. The signal waveforms shown in these figures are for SEs and BSEs. For BSE two types of signals are presented. One is the whole amount of BSEs emitted from the specimen surface after all kinds of reentries of electrons to the specimen, and another is only the amount of emitted BSEs flying toward a limited region of the detector. We assumed this detector to have a circular shape with a radius of 10mm, set 10mm above the specimen surface C. This boundary condition is determined supposing the detector is set at the bottom of the pole piece of the objective lens in the SEM with the working distance of 10mm. The amount of the signal is expressed in terms of those yields. On these graphs, lines are drawn connecting the points obtained by calculation. Although they include some statistical errors, they allow quantitative discussion of the changes in SE signals and BSE signals which are known as topographic contrast. For example, quantitative discussions can be made over the difference of signal between the A-B edge and the B-C edge as follows.

In this calculation, the edge effect is reinforced by the phenomenon that the signal on the plane area of A and C (in particular that of SEs) becomes smaller as the energy of PEs increased. This finding is consistent with the reported phenomenon of SEM that the elevation of the acceleration voltage results in emphasis of the image contrast. Furthermore, as the energy of PEs becomes larger, the rise of the SE and BSE signals in the vicinity of the edge becomes dull. This finding suggests that the resolution of SEM decreases at high acceleration voltages. This phenomenon has also been observed in a practical use of the SEM.

Fig.17(a-f) is an enlarged presentation of Figs.15(a-c), and Figs.16(a-c) for 1 and 3 keV PEs, respectively, for the changes in signal of SE and BSE at the vicinity of the edge when the side wall of the pattern stands vertically. Assuming a PE trajectory as that, PE enters the surface A

Table III. Distance from the A-B edge to the site of the maximum signal for SE, total emitted BSE, and detected BSE.

	1keV	3keV
SE (δ)	1.0 nm	1.0 nm
BSE (η_1)	0.3 nm	0.2 nm
BSE (η_2)	0.3 nm	0.1 nm

Table IV. Full width at half maximum of the distribution of the rise signal at A-B edge from the signal at the surface A.

	1keV	3keV
SE (δ)	3.71 nm	6.72 nm
BSE (η_1)	2.52 nm	~ 14.0 nm
BSE (η_2)	0.99 nm	~ 9.0 nm

Table V. Distance from the B-C edge to the site of the mimimum signal for SE, total emitted BSE, and detected BSE.

	1keV	3keV
SE (δ)	$\leq$ 0.01 nm	0.1 nm
BSE (η_1)	$\leq$ 0.01 nm	$\leq$ 0.01 nm
BSE (η_2)	$\leq$ 0.01 nm	0.1 nm

Table VI. Full width at half maximum of the distribution of the fall signal at B-C edge from the signal at the surface C.

	1keV	3keV
SE (δ)	0.62 nm	2.08 nm
BSE (η_1)	0.47 nm	5.41 nm
BSE (η_2)	0.45 nm	4.71 nm

at a point near the edge, goes out of the surface B and reenters the surface C, SEs emit from the surfaces A, B, and C close to the points of PEs' incidence, exit, and the reentry, respectively. Therefore, the signal of SEs is maximal when the PEs have traveled the most efficient path to produce SEs within the SE escape length measured toward inside normal to each surface. Hence, the maximum SE signal intensity is obtained at a point slightly off the edge toward the surface A instead of at a point right over the edge. There has been a difficulty in a quantification of the SE intensity at the edge in numerical calculations, unless individual SE trajectory has been calculated as in the present simulation. Previous treatment of the SE signal using the amount of PE energy deposition in a specimen seems to be insufficient in the estimation of the value.[20,22,37,48,49] On the other hand, the contribution of PE reentry onto the surface C to the BSE signal can be regarded as small, as discussed in the last paragraph. Therefore, the maximum BSE signal is seen in the vicinity of the edge in most cases. The offset for each maximum signal of SE, BSE, and detected BSE from the A-B edge is summarized in Table III. The full width at half maximum of each distribution of the rise signal from the signal at the surface A in the vicinity of A-B edge is summarized in Table IV.

For both SE and BSE, a fall of signal at the B-C edge is observed. As the energy of PEs increases, the fall becomes smaller, and the fall in the vicinity of this edge becomes less sharp like we have seen in the signals for the A-B edge. Tables V and VI show the distance from the edge to the site of the minimum signal and the full width at half maximum of the distribution of the fall of signal from the signal at the surface C. Since the value in Table V is so low, the statistics is not good. Here, the distance between the A-B edge and the site of maximum signal is much larger than that between the B-C edge and the site of minimum signal. Also, the full width at half maximum of the rise distribution at A-B edge is much wider than that of the fall distribution at B-C edge. This is because the influence of the electron reentry to the signal is not so large at the B-C edge and the signals depend primarily on the oblique angle of the specimen to the primary beam.

In the above calculations, we assumed that the diameter of electron beams is zero. In spite of this assumption, the maximum signal intensity does not coincide with the topographic edge. This result indicates the necessity for us to be careful in determining the absolute size of fine structures using the SEM.

To compare the signal intensity between SE and BSE, it is lower for BSE at every combination. In addition, the contrast at the edge is clearer for SE. The BSE signal intensity η_2, which takes into consideration the presence of a detector, is generally much smaller than others because the detected solid angle is small. This signal shows almost no rise at the surface B. This is because the intensity of BSEs which take trajectories of direction almost opposite to the electron beam does not change so much by the inclination of the specimen surface, as shown in the calculation by Reimer and Stelter.[41] Many of the BSEs, which are scattered at such a large angle from the specimen, have suffered large angle (almost 180 degree) single scattering in the first or the second step of PEs in the specimen, and this phenomenon does not depend on the inclination of the specimen surface, but primarily depend on the differential cross section of the elastic scattering used in the single scattering model.

Conclusion

A new Monte Carlo calculation model is proposed to simulate not only the primary electron behavior but also the secondary electron cascade in a specimen. Calculated physical quantities agree well with the experimental results. The theoretical spatial resolution of SE and BSE images in the SEM are obtained. The present calculation makes it possible to simulate the SEM image utilizing either SE or BSE signal. Future studies should be made in which the present simulation is applied to various features of the specimen in order to determine the contrast and resolution that can be theoretically obtained.

In scanning electron microscopy, the scattering of electrons produce signals of complicated contrasts which are affected not only by the inclination on the specimen's surface but also by the following factors: (1)the relationship between the length of the inclined area of a specimen and the range of PE diffusion in the specimen, and (2)the effect of the electron reentries onto the specimen after they are once emitted from the specimen. In this paper, an analysis of the SEM images is presented using the recently developed Monte Carlo simulation. Many features of SEM image will be studied in future.

References

1. Alig RC, Bloom S. (1978). Secondary-electron-escape probabilities. J. Appl. Phys.,49, 3476-3480.

2. Amelio GF. (1970). Theory for the energy distribution of secondary electrons. J. Vac. Sci. Technol., 7, 593-604.

3. Bennett AJ, Roth LM. (1972). Effect of primary-electron diffusion on secondary-electron emission. Phys. Rev. B, 5, 4309-4324.

4. Berger MJ, Seltzer SM. (1964). Tables of energy-losses and ranges of electrons and positrons. Natl. Acad. Sci. Natl. Res. Council 1133, 205-268 (Washington, D.C.).

5. Bindi R, Lantéri H, Rostaing P. (1980). Application of the Boltzmann equation to secondary electron emission from copper and gold. J. Phys. D 13, 461-470.

6. Bindi R, Lantéri H, Rostaing P, Keller P. (1980). Theoretical efficiency of back-scattered electrons in secondary electron emission from aluminium. J. Phys. D 13, 2351-2361.

7. Bindi R, Lantéri H, Rostaing P. (1987). Secondary electron emission induced by electron bombardment of polycrystalline metallic targets. Scanning Microscopy, 1, 1475-1490.

8. Bonham RA, Strand TG. (1963) Analytical expressions for potentials of neutral Thomas-Fermi-Dirac Atoms and for the corresponding atomic scattering factors for X rays and electrons. J. Chem. Phys., 39, 2200-2204.

9. Bronshtein IM, Fraiman BS. (1961). Inelastic scattering of electrons and secondary electron emission from certain metals and semiconductors. Sov. Phys. Solid State,3, 1188-1196.

10. Bühring W. (1968). Elastic Electron Scattering by Mercury Atoms. Z. Phys., 212, 61-70.

11. Bunyan PJ, Schonfelder JL. (1965). Polarization by mercury of 100 to 2000eV electrons. Proc. Phys. Soc., 85, 455-462.

12. Byatt WJ. (1956). Analytical representation of Hartree potentials and electron scattering. Phys. Rev., 104, 1298-1300 (1956).

13. Cailler M, Ganachaud JP. (1983). A simulation model for the secondary electron emission from metals. Application to the study of the Auger electron emission of aluminium. Scanning Electron Microsc. 1983; I: 85-97.

14. Chung MS, Everhart TE. (1974) Simple calculation of energy distribution of low-energy secondary electrons emitted from metals under electron bombardment. J. Appl. Phys., 45, 707-709.

15. Chung MS. (1975). Improved calculations of secondary electron energy distributions of metals. J. Appl. Phys., 46, 465-466.

16. Ding Z-J, Shimizu R. (1988). Monte Carlo study of backscattering and secondary electron generation. Surf. Sci. 197, 539-554.

17. Ganachaud JP, Cailler M. (1973). Traitement Unifié de L'Émission Électronique Secondaire de Cuivre par une Méthode de Monte Carlo. J. de Phys., 34, 91-98.

18. Ganachaud JP, Cailler M, Aberdam D, Blanc E, Gaubert C. (1979). New theoretical results about the anisotropy of the secondary emission of Al(001) and Al(110). Surf. Sci., 87, 129-140.

19. Ganachaud JP, Cailler M. (1979). A Monte-Carlo calculation of the secondary electron emission of normal metals Surf. Sci., 83, 498-530.

20. George EP, Robinson VNE. (1976). The dependence of SEM contrast upon electron penetration. Scanning Electron Microscopy 1976; I: 17-26.

21. Horgues CD, Ganachaud JP, Cailler M. (1976). A simulation of the transmission of 1keV electrons through thin films of aluminum, copper and gold. J. Phys. D 9, L633-L636.

22. Joy DC. (1988). Image simulation for secondary electron micrographs in the scanning electron microscope. Scanning Microscopy, 2, 57-64.

23. Kaczmarek D, Czyzewski Z. (1988). Signal of backscattered electrons from multiple marks in dependence on mark profile. Scanning Microscopy, 2, 1273-1281.

24. Kanaya K, Kawakatsu H. (1972). Secondary electron emission due to primary and backscattered electrons. J. Phys. D 5, 1727-1742.

25. Koshikawa T, Shimizu R. (1973). Secondary electron and backscattering measurements for polycrystalline copper with a spherical retarding-field analyser. J. Phys. D 6, 1369-1380.

26. Koshikawa T, Shimizu R. (1974). A Monte Carlo calculation of low-energy secondary electron emission from metals. J. Phys. D 7, 1303-1315.

27. Koshikawa.(1973). Secondary electron emission in surface analysis (in Japanese). Thesis, Osaka University. p.64.

28. Kotera M, Murata K, Nagami K. (1981). Monte Carlo simulation of 1-10-keV electron scattering in a gold target. J. Appl. Phys., 52, 997-1003.

29. Kotera M, Murata K, Nagami K. (1981). Monte Carlo simulation of 1-10-keV electron scattering in an aluminum target. J. Appl. Phys., 52, 7403-7408.

30. Kotera M, Kishida T. (1989) A Monte Carlo simulation of secondary electron trajectories in a specimen. Jpn. J. Appl. Phys. 28, 148-149.

31. Kotera M. (1989) A Monte Carlo simulation of primary and secondary electron trajectories in

a specimen. J. Appl. Phys. 65, 3991-3998.

32. Lin SR. (1964). Elastic electron scattering by screened nuclei. Phys. Rev., 133, A965-A970.

33. Lin YC, Adesida I, Neureuther AR. (1980). Monte Carlo simulation of registration signals for electron beam microfabrication. Appl. Phys. Lett. 36, 672-674.

34. Luo S, Joy DC. (1988). Monte Carlo calculations of secondary electron emission. Scanning Microscopy, 2, 1901-1915.

35. Lye RG, Dekker AJ. (1957). Theory of secondary emission. Phys. Rev., 107, 977-981.

36. Makarov VV, Petrov NN. (1981). Regularities of secondary electron emission of the elements of the periodic table. Sov. Phys. Solid State, 23, 1028-1032.

37. Murata K, Kawata H, Nagami K. (1987). Electron scattering in low voltage scanning electron microscope targets. Scanning Microscopy, Suppl. 1, 83-91.

38. Niedrig H. (1982). Analytical models in electron backscattering, in: Electron Beam Interaction with Solids, D.F.Kyser, H.Niedrig, D.E.Newbury, and R.Shimizu (ed), Scanning Electron Microsc., Chicago, 51-68.

39. Ono S, Kanaya K. (1972). The energy dependence of secondary emission based on the range-energy retardation power formula. J. Phys. D 12, 619-632.

40. Rao Sahib T, Wittry DB. (1974). X-ray continuum from thick elemental targets for 10-50keV electrons. J. Appl. Phys., 45, 5060-5068.

41. Reimer L, Stelter D. (1981). Monte Carlo calculations of electron emission at surface edges. Scanning Microscopy, 1, 951-962.

42. Rosenfield MG, Neureuther AR, Viswanathan R. (1983). Simulation of backscattered electron signals for x-ray mask inspection. J. Vac. Sci. Technol. B, 1, 1358-1363 (1983).

43. Salehi M, Flinn EA. (1980). An experimental assessment of proposed universal yield curves for secondary electron emission. J. Phys. D 13, 281-289.

44. Schou J. (1980). Transport theory for kinetic emission of secondary electrons from solids. Phys. Rev. B, 22, 2141-2174.

45. Schou J. (1988). Secondary electron emission from solids by electron and proton bombardment. Scanning Microscopy, 2, 607-632.

46. Seiler H. (1963). Einige aktuelle Probleme der Sekundarelektronenemission. Z. Angew. Phys., 22, 249-263.

47. Seiler H. (1983). Secondary electron emission in the scanning electron microscope. J. Appl. Phys., 54, R1-R18.

48. Shimizu R, Murata K. (1971). Monte Carlo calculations of the electron-sample interactions in the scanning electron microscope. J. Appl. Phys., 42, 387-394.

49. Shimizu R. (1974). Secondary electron yield with primary electron beam of kilo-electron-volts. J. Appl. Phys., 45, 2107-2111.

50. Stephani D. (1979). Monte-Carlo calculations of backscattered electrons at registration marks. J. Vac. Sci. Technol., 16, 1739-1742.

51. Strand TG, Bonham RA. (1964). Analytical expressions for the Hartree-Fock potential of neutral atoms and for the corresponding scattering factors for x rays and electrons. J. Chem. Phys., 40, 1686-1689.

52. Streitwolf HW. (1959). Zur Theorie der Sekundarelektronenemission von Metallen der Anregungsprozess. Ann Phys. (Leipz.), 3, 183-196.

53. Wolff PA. (1954). Theory of secondary electron cascade in metals. Phys. Rev., 95, 56-66.

54. Yamazaki Y. (1977). Studies on Electron Scattering by Mercury Atoms and Electron Spin Polarization detector. Doctorate Thesis, Osaka University.

Discussion with Reviewers

D.C.Joy : While the use of the elastic mean free path as the determining quantity for the step length is appropriate when considering the primary electron scattering, it would surely be more correct to use the total mean free path (elastic and inelastic) when considering secondary electron production (see for example Shimizu et al, J. Phys. D9, 101, 1976).

Authors : In the present study as described in the text, we used two different models depending on the electron energy. Because of this, it is not necessary to use "the total mean free path" in the simulation as explained in the following. For a fast electron we used the single scattering model and no inelastic scattering is considered; the angular scattering of fast electrons is determined only by the elastic scattering. For a slow electron we used the cascade model and no elastic scattering is considered; the angular scattering is determined only by the electron-electron (binary) scattering. The single scattering model has been widely accepted (see for example NBS Spec. Publ. 460, 1976) in the field of e.g. electron probe micro-analysis, because it gives quite reasonable results for fast electron (>100eV) energy deposition in a specimen. The reason why the model gives reasonable results is that an average energy loss in a step ($\simeq$ elastic scattering mean free path) is much smaller than the energy of the fast electron, and the scattering angle by the inelastic collision is small. On the other hand, for slow electrons (<100eV) a major mechanism in producing SEs in metals is the electron cascade process. As a matter of course, elastic scattering cross section is quite large, but the major role is to make electron trajectory more random. As far as the angular distribution is concerned, the calculated distribution of emitted SEs at the specimen surface shows a cosine distribution, and this proves that the SE trajectory in the specimen is almost random. Then, it may not be quite important to take into account the elastic scattering cross section in the treatment of slow electrons. In these physical aspect we divide electrons into two kinds; fast and slow electrons. Under this assumption, we do not do the so called direct simulation which Shimizu, Kataoka, Ikuta, Koshikawa, and Hashimoto have done, and "the total mean free path" is not necessary to use in the present simulation.

D.C.Joy : The use of the Rao-Sahib Wittry stopping power extrapolation at low energies is a significant inaccuracy. It would be better to use the

tabulated data from Tung et al.(as was done in the recent paper by Ding and Shimizu, J. Microsc. 154, 193 (1989)) or an improved analytical expression).
Authors : Tung, Ashley, and Ritchie obtained the stopping power using the dielectric function with some corrections for the conduction electron contribution, and the generalized oscillator strength function for the contribution of inner-shell electron ionization. In one of two approaches of Ding and Shimizu's paper the Tung et al.'s calculation is used for the total stopping power. They gave another approach which was using the dielectric function with their own modification. The stopping power we used here is very close to that of Tung et al. in a whole range of energy down to the cut off energy (=11.45eV). In the present model we used the Rao-Sahib Wittry equation down to 100eV. Although the overestimation of the stopping power is appreciable below 500eV, the distance an electron at 500eV can travel is only about 5nm until its energy is 100eV. Below 100eV we used the mean free path of cascade scattering, and the energy dependence is expressed in Eq.(28). Because we incorporate two models as described in the text, the stopping power we used is not so inaccurate. (see our recent paper in Scanning Microsc.3(4), 1989)

Stopping power, which Tung et al., and some others have derived is only an average energy loss of a primary electron divided by its mean free path in one electron-electron collision, and it is an expression for convenience. Depending on the energy region of interest, simulation models can be constituted. However, if we consider the inelastic collision at low energy region (<100eV), the value of the stopping power itself is meaningless. In other words, if we consider slow electrons, the value of the energy transfer at every collision should be taken into account and the trajectory of electrons which obtains the transferred energy should be traced. Also, we have to note that the distribution of transferred energy is different depending on each type of collision.

D.C.Joy : Most authors have chosen λ_i to be specimen dependent. The choice of an material independent model for λ_i is a possible source of inaccuracy.
Authors : The experimental value of λ_i is widely scattered as found for example in the figures of Tung et al's paper. The deviation is sometimes 100% for Al, Si or Ni, and for other materials we have to point out that the number of experimental points is too small. In analytical expressions, it is surely possible to include the material dependences. However, on the other hand, the difference among the theoretical values of Tung et al. for Al, Si, Cu, Ag and Au is almost less than 30%. It should be pointed out that it is quite difficult to define the real accurate value for the inelastic mean free path at present. In the present simulation we take into account the step length straggling with a random number as in Eq.(23), and the deviation of our value as expressed in Eq.(28) from the theoretical value is almost covered by this straggling distribution.

D.C.Joy : The assumption that the cascade model need not consider energies above 100eV is not obviously correct. Other workers (Ding and Shimizu 1989, Luo and Joy 1988, text ref.34) have shown that the higher energy secondaries do still make a significant contribution.
Authors : As described in the text (see the explanation for Fig.2), we consider fast electron generations from fast electron (which may be primary electron or generated fast electron) trajectories. This is apparently the cascade process of fast electrons.

D.E.Newbury : What is the valid energy range for the Streitwolf equation?
Authors : There is no limitation in the use of the Streitwolf equation in energy, and it has been used by Shimizu's group (for example, Koshikawa and Shimizu, text ref.26, Shimizu et al., J. Phys. D9, 101(1976), Shimizu and Ichimura, Proc. 1st Pfefferkorn Conf. SEM 165 (1982), etc.). However, this equation is originally derived for simple metals, not for transition metals, and the screening effect of the electronic charge by electron gas (plasma) is not considered. It is quite easy to use but for a discussion in detail it is necessary to know its limitation.

D.E.Newbury : Is there a fundamental reason why the energy loss associated with fast secondary electron production is neglected?
Authors : In the present calculation, first, PE trajectory is calculated and the deposited energy in the specimen is obtained. Depending on the amount of energy deposited, number of SEs generated is determined. The generated SE has a energy distribution as described by the Streitwolf equation. Since the calculation has been done in this sequence, it was impossible to consider the energy loss of fast electrons associated with fast secondary electron production. New computer code will appear soon.

J.P.Ganachaud : Is the scattering function plotted in Fig.7 strictly null for angles greater than 90 degree?
Authors : No, but since the value of the function greater than 90 degree is 2 to 3 orders of magnitude less than that of the forward scattering, it disappears in the linear plot.

M.Cailler : How many d-band electrons are taken into account in the simulation?
Authors : Since we used the value E_F=7.0, the number of conduction band electrons considered is one, and no contribution of d-band electrons is taken into account. Whereas, in the present approach, irrespective of the value of the Fermi energy, total secondary yield is set to agree with the experimental data, the resultant calculated yields do not depend primarily on the number of d-band electrons considered. As the second order effect of taking different E_F, the shape of energy distribution of SE changes.